Ionization Dynamics of the Branched Water Cluster: A Long-lived Non-Proton-transferred Intermediate

Hiroto TACHIKAWA*[a] and Tomoya TAKADA[b]

[a]*Division of Materials Chemistry, Graduate School of Engineering, Hokkaido University, Sapporo 060-8628, Japan*

[b]*Department of Bio- and Material photonics, Chitose Institute of Science and Technology, Bibi, Chitose 066-8655, Japan*

Manuscript submitted to: *Computational and Theoretical Chemistry*
Section of the journal: *Article*
Running title: *Reaction rate of proton transfer*

Correspondence and Proof to: Dr. Hiroto TACHIKAWA*
Division of Materials Chemistry
Graduate School of Engineering
Hokkaido University
Sapporo 060-8628, JAPAN
hiroto@eng.hokudai.ac.jp
Fax +81 11706-7897

Contents:

Ionization Dynamics of the Branched Water Cluster: A Long-lived Non-Proton-transferred Intermediate

Authors: **Hiroto TACHIKAWA*[a] and Tomoya TAKADA[b]**

[a]Division of Materials Chemistry, Graduate School of Engineering, Hokkaido University, Kita-ku, Sapporo 060-8628, Japan
[b]Department of Bio- and Material photonics, Chitose Institute of Science and Technology, Bibi, Chitose 066-8655, Japan

Abstract: The proton transfer (PT) reaction after water cluster ionization is known to be a very fast process occurring on the 10-30 fs time scale. In the present study, the ionization dynamics of the branched water tetramer $(H_2O)_4$ were investigated by means of a direct ab initio molecular dynamics (AIMD) method to elucidate the time scale of PT in the water cluster cation. A long-lived non-proton-transferred intermediate was found to exist after the ionization of the branched-type water cluster. The lifetimes of the intermediate were calculated to be ca. 100-150 fs. PT occurred after the formation of the intermediate. The structure of the intermediate was composed of a symmetric cation core: H_2O-H_2O^+-H_2O. The broken symmetry of the structure led to PT from the intermediate. The reaction mechanism is discussed based on the theoretical results.

Keywords: ab initio MD; lifetime; water tetramer; reaction rate

1. Introduction

Irradiation by cosmic rays and sunlight ionizes the water ice surrounding icy planets. Subsequently, several reaction processes compete with each other. First, an excess electron derived from the water cluster is solvated by surrounding water molecules, resulting in the formation of a hydrated electron, $e^-(H_2O)_n$. Additionally, the ionized water molecule (H_2O^+) reacts with its surrounding water molecules. In this case, the most typical reaction is a proton transfer (PT) from H_2O^+ to H_2O: $H_2O^+ + H_2O \rightarrow H_3O^+ + OH$.

The PT process plays an important role in astrophysics and biochemistry. Therefore, pure and protonated water clusters [1-8] and solute-water clusters [9-22] have been investigated both experimentally and theoretically. The photo-ionization of large-sized water clusters has been studied using several experimental techniques [23-26]. The reaction processes of a water cluster after ionization can be summarized as follows:

$$(H_2O)_n + Ip \rightarrow [(H_2O)_n^+]_{VER} + e^- \quad \text{(ionization)}$$

$$[(H_2O)_n^+]_{VER} \rightarrow (H_3O^+)(OH)(H_2O)_{n-2} \quad \text{(complex formation)}$$

$$\rightarrow H^+(H_2O)_{n-1} + OH \quad \text{(OH dissociation)}$$

$$\rightarrow H^+(H_2O)_{n-k} + (k-1)H_2O + OH \quad \text{(OH dissociation + } H_2O \text{ evaporation)}$$

where IP and VER represent the ionization potential and vertical ionized state from the neutral cluster, respectively. The first channel corresponds to complex formation: The ion-radical pair with a $(H_3O^+)OH$ core forms after PT from H_2O^+ to H_2O. The second and third channels correspond to OH dissociation from the cluster and three-body dissociation, respectively. In all channels, PT occurs first: $H_2O^+ + H_2O \rightarrow H_3O^+ + OH$. Although the existing knowledge of the final products was accumulated via

experimental and theoretical works, the mechanism of the first PT process is not completely understood. In particular, very little information exists regarding the time scale of the first PT.

In previous papers, we studied the ionization processes of small-sized water clusters using a direct ab initio molecular dynamics (AIMD) method [27]. Water dimers (n=2), trimers (n=3), and cyclic tetramers (n=4) were examined as the water clusters, where *n* represents the number of H_2O molecules in the clusters, and the PT reaction rates in the water cluster cation $(H_2O)_n^+$ (n=2-4) were determined. The calculations revealed that the PT reaction rates are 28 fs (*n*=2), 15 fs (*n*=3), and 10 fs (*n*=4). These results suggested that PT in the water cluster cation is a very fast process and proceeds directly without the formation of an intermediate [28,29]. Previously, only the cyclic form of the water tetramer was examined theoretically.

In the present study, the ionization dynamics of the branched water tetramer, the smallest water cluster possessing the branched from, were investigated theoretically to elucidate the effects of the cluster's structural form on the PT dynamics in water clusters. The direct AIMD method was applied to the ionization dynamics of water tetramers with both branched and cyclic forms. Here, the PT reaction rates and the lifetimes of the intermediate complex were compared.

2. Calculation method

2.1. Static ab initio calculations

Static ab initio calculations were conducted using the Gaussian 09 program package and the 6-311++G(d,p) and aug-cc-pVTZ basis sets.[30] The geometries and energies were obtained by MP2 and MP4SDQ methods. The atomic charge was calculated using

natural population analysis (NPA).

2.2. Direct AIMD calculations from the optimized structures

In the direct AIMD calculation [31-36], the geometry of the neutral cluster $(H_2O)_4$ was fully optimized at the MP2/6-311++G(d,p) level. The trajectory on the ionic state potential energy surface was started from the equilibrium point of the parent neutral $(H_2O)_4$ cluster. Both velocities of all atoms and the angular momenta were set to zero at time zero. Additionally, the excess energy of the system at time zero was fixed to zero. The equation of motion was solved by the velocity Verlet algorithm with a time step of 0.1 fs. We carefully checked that the drift of the total energy (potential energy plus kinetic energy) was less than 0.01 kcal/mol in all trajectories. No symmetry restriction was applied to the calculation of the energy gradients.

The relation of the total, potential, and kinetic energies is expressed by

$$E(total) = E(kinetic) + E(potential).$$

Because we used the microcanonical ensemble (NVE ensemble) in the AIMD calculations, the total energy of the reaction system was constant during the simulation.

In addition to the MP2 geometries of $(H_2O)_4$, the optimized structures obtained by QCISD/6-311++G(d,p) and MP4SDQ/6-311++G(d,p) were examined as starting $[(H_2O)_n^+]_{ver}$ geometries in the direct AIMD calculations to elucidate the effects of the initial geometry on the PT reaction rate. Note that these calculations gave the similar results for the reaction dynamics.

2.3. Direct AIMD calculations from Franck-Condon region

In addition to the trajectories from the optimized geometries, the trajectories around

the equilibrium point were also calculated. Two sampling methods—Franck-Condon (FC) and thermal sampling—were used to obtain the initial geometries at time zero. A total of 30 trajectories were run.

In the FC sampling, the selected geometries in the FC region were chosen as follows: First, the structure of $(H_2O)_4$ was fully optimized at the MP2/6-311++G(d,p) level of theory. Next, the geometries were generated around the equilibrium point: the intermolecular distances between water molecules were changed by ±0.10 Å. The total energy and optimized structure of $(H_2O)_4$ are expressed by $E_0(n)$ and $[(H_2O)_4]_0$, respectively. Second, the geometries of $(H_2O)_4$ around the equilibrium points of $[(H_2O)_4]_0$ were generated. We changed the intermolecular distances between water molecules in the generation of initial geometries. The generated geometries are expressed by $[(H_2O)_4]_i$, and their total energies are expressed by $E_i(n)$, where ***i*** indicates the number of the generated configuration of $[(H_2O)_4]_i$. Third, the energy difference between E_i and E_0 was calculated as $\Delta E_i = E_i - E_0$. We selected generated geometries with ΔE_i less than 1.0 kcal/mol ($\Delta E_i < 1.0$ kcal/mol) as the starting points for the direct AIMD calculations. The trajectory calculations of $(H_2O)_4^+$ were performed under the constant total energy condition at the MP2/6-311++G(d,p) level. The velocity of each atom was set to zero at time zero.

2.4. Direct AIMD calculations from thermal activation region

In the thermal sampling, the structure of $(H_2O)_4$ was first optimized at the B3LYP/6-311++G(d,p) level. The structure of $(H_2O)_4$ was fluctuated at 10 K using B3LYP/6-311++G(d,p) MD simulation. Starting from the optimized geometry, we carried out the direct AIMD calculation under the constant temperature condition [37]

and used 10 K as the average temperature. The atom velocities at the starting point were adjusted to the selected temperature. To maintain a constant temperature in the system, bath relaxation time was introduced into the calculation. We applied the Berendsen thermostat [38-41] to the trajectory calculations under the chosen thermal conditions.

Geometries were selected based on the trajectory calculations at 10 K. This temperature corresponded to that in interstellar space and ice of comets. The trajectories on the ionic state potential energy surface of $(H_2O)_4^+$ were run using the assumption of vertical ionization from the neutral state. The trajectory calculations of $(H_2O)_4^+$ were performed under the constant total energy condition at the MP2/6-311++G(d,p) level. A total of 30 trajectories were run in the thermal sampling. Details of sampling methods were described in our recent paper [42].

3. Results

A. Structures of the branched water tetramer

First, the geometries of the branched water tetramer $(H_2O)_4$ were fully optimized at three levels of theory. The structures obtained are illustrated in Figure 1. The branched water tetramer was composed of cyclic water molecules (W1, W2, and W3) and one attached water molecule (W4). One water molecule (W1) was located in the central region of the cluster and was connected to the other three water molecules (W2, W3, and W4). The hydrogen bond distances were calculated to be 2.011 Å (W1-W2), 1.856 Å (W1-W3), 1.939 Å (W1-W4), and 1.906 Å (W2-W3), indicating that the bond distances differed from each other. According to the NPA calculations, the molecular charges on the water molecules were close to zero.

At the vertical ionization state, the spin densities of the water molecules of the

branched form at time zero were calculated to be 0.99 (W1), 0.00 (W2 and W4), and 0.01 (W3) at the MP2/6-311++G(d,p) level. The spatial distribution of the spin orbital of the water tetramer cation is illustrated in Figure 1B, and the spin orbital was mainly localized on W1. Similar geometrical features and electronic states of the $(H_2O)_4$ system were obtained at the MP4SDQ/6-311++G(d,p) level.

B. Ionization dynamics of the branched water tetramer (*n*=4)

Snapshots

Snapshots of the $(H_2O)_4^+$ cation after vertical ionization of the branched water cluster are illustrated in Figure 2. The structure was optimized at the MP2/6-311++G(d,p) level. A hole was mainly localized on W1, which is located in the center of the branched form. A repulsive interaction formed rapidly between $W1^+$ and a proton of W3 (the displacements are indicated by arrows), causing W3 to move away from $W1^+$ and rotate.

The hydrogen bond distances were 2.011 Å (W1-W2), 1.906 Å (W2-W3), 1.856 Å (W1-W3), and 1.939 Å (W1-W4) at time zero. The oxygen-oxygen distance (W1-W2) was 2.857 Å. At 26 fs, W3 moved gradually away from $W1^+$ (oxygen-oxygen distance of 2.841 Å for W1-W2) because of the repulsive interaction. A non-proton-transferred intermediate composed of H_2O(W4)-H_2O^+(W1)-H_2O(W2) formed. Both W2 and W4 were located almost equidistantly from $W1^+$. At 47 fs (point **c**), the proton still had not been transferred, and it existed as a hydrated H_2O^+ in the center of W2-W4. At 127 fs, the proton transferred from $W1^+$ to W2, forming the H_3O^+(OH) complex (403 fs). Finally, the second PT occurred from W2(H^+) to W4 at 500 fs.

Potential energy

The time propagations of the potential energy of the branched form after ionization are given in Figure 3A. The zero level of the energy corresponds to that of $[(H_2O)_4^+]_{VER}$ at the point of vertical ionization from the neutral tetramer (point **a**). After the ionization of $(H_2O)_4$, the energy decreased gradually to –31 kcal/mol at 29 fs (point **b**) because of the structural relaxation of $W1^+$. Solvent re-orientation occurred immediately around $W1^+$ (50-100 fs). The intermediate complex with a H_2O^+ core solvated by two water molecules formed between 26 and 127 fs. The proton of $W1^+$ was not transferred at this time, but at 127 fs, PT was completed.

For comparison, the ionization dynamics of the cyclic tetramer was also investigated in the same manner. The cyclic tetramer was stable in energy than that of branched tetramer (-7.0 kcal/mol). Figure 3B shows the time evolution of the water cation in the cyclic form. The first PT occurred at 7 fs, which is approximately 10 times faster than that of the branched form. The potential energy decreased rapidly to –38 kcal/mol (7 fs) and then to –40 kcal/mol (12 fs). This decrease in energy was caused by the first PT from $W1^+$ to W2. The second PT was completed at 37 fs, and at this point, the OH radical dissociated from the system. Thus, the time scales of PT and the reaction processes of the branched and cyclic forms differ significantly from each other.

C. Summary of the direct AIMD calculations

A total of 30 trajectories were run from the selected points in the FC region. The average of PT reaction rate (PT rate) is given in Table 1 together with the average value of PT in the cyclic form. The reaction rates obtained for the branched and cyclic forms were 125 and 10 fs, respectively. Additionally, the reaction rate obtained by thermal

sampling (120 fs) is also given in Table 1. All the calculations indicate that the PT rate in the branched form (ca. 125 fs) is significantly slowly than that of the cyclic form (10 fs) and that a non-proton-transferred intermediate was formed during this process in the branched form. In contrast, PT proceeded directly without complex formation in the cyclic form, and all trajectories gave the OH dissociation product as the final state.

Table 1. PT reaction rates (in fs) obtained from several direct AIMD calculations.

Conformer (method)	PT rate
branched (MP2 opt. geom.) [a]	127
branched (FC sampling) [a]	125
branched (10K sampling) [b]	120
branched (MP4SDQ opt. geom.) [c]	105
branched (QCISD opt. geom.) [d]	124
branched (B3LYP opt.geom.) [e]	115
cyclic (MP2 opt. geom.) [a]	12
cyclic (10K sampling) [b]	10

[a] The geometry was optimized at the MP2/6-311++G(d,p) level, and the AIMD was carried out at the MP2/6-311++G(d,p) level.
[b] The geometries were generated by thermal MD calculation (10 K) at the B3LYP/6-311++G(d,p) level and the AIMD was carried out at the MP2/6-311++G(d,p) level.
[c] The geometry was optimized at the MP4SDQ/6-311++G(d,p) level, and the AIMD was carried out at the MP2/6-311++G(d,p) level.
[d] The geometry was optimized at the QCISD/6-311++G(d,p) level, and the AIMD was carried out at the MP2/6-311++G(d,p) level.
[e] The geometry was optimized at the B3LYP/6-311++G(d,p) level, and the AIMD was carried out at the B3LYP/6-311++G(d,p) level.

D. Structure of the intermediate complex

The dynamics calculations revealed that a long-lived intermediate forms before the PT in the branched form but not in the cyclic form. In the branched from, the hole was localized on the center position among the three water molecules: H_2O-H_2O^+-H_2O. This cation core complex subsequently evolved to become the intermediate complex with a core cation and a symmetric structure in which the protons of H_2O^+ orient equivalently to both surrounding H_2O molecules. Therefore, this structure inhibits PT.

To elucidate the existence of the intermediate in more detail, the geometry of the intermediate, H_2O-H_2O^+-H_2O, was fully optimized at the MP2/6-311++G(d,p) level, and the result is given in Figure 4, together with the non-proton transferred intermediate with n=4. All of the vibrational frequencies calculated for $(H_2O)_3$, $(H_2O)_3^+$, and $(H_2O)_4^+$ were positive, indicating that the optimized structures are located at local minima on the potential energy surface.

In the neutral water trimer, the hydrogen bond distances and H-O-H bond angle were 1.999 Å and 104.2º, respectively. In the intermediate complex $(H_2O)_3^+$, the water molecule in the central region was locally ionized. The hydrogen bond distance was 1.383 Å, which is significantly shorter than the normal hydrogen bond (1.383 vs. 1.999 Å). The H-O-H angle of H_2O^+ in the intermediate was 114.9º, indicating that the structure of the H_2O^+ moiety is substantially deformed by the hole capture. The product structure of $(H_2O)_3^+$ after intra-cluster PT from H_2O^+ to H_2O is illustrated in Figure 4C. The energy difference between the intermediate and product states was calculated to be only 4.4 kcal/mol. Similar results were obtained at the MP4SDQ/6-311++G(d,p) level. The energy level of the intermediate is extremely close to that of the product state, and

thus, its lifetime is extended. The structure of non-proton transferred intermediate of *n*=4 is significantly different from the cation core in *n*=3.

E. Lifetime of intermediate complex

To investigate the long lifetime of the symmetric intermediate H_2O-H_2O^+-H_2O, AIMD calculations were conducted for the linear water trimer. First, the geometry was fully optimized at the MP2/6-31++G(d,p) level. All the vibrational frequencies of $(H_2O)_3$ were positive, indicating that the structure of $(H_2O)_3$ is located at a local minimum on the potential energy surface. The trajectory was started from the optimized structure with the assumption of vertical ionization. No symmetry restriction was employed. The time evolution of the potential energy and snapshots of $(H_2O)_3^+$ are given in Figure 5. After ionization, the potential energy decreased to –20 kcal/mol because of the structural deformation of H_2O^+, and it periodically vibrated. A long-lived intermediate was formed. The simulation was extended to 400 fs, but the proton was never transferred. These calculations confirmed that the intermediate's lifetime exceeds 400 fs and suggest that the long-lived complex can take the form of H_2O-H_2O^+-H_2O.

F. Ionization process of a cage-type water hexamer

The present study showed that both fast and slow PT processes are possible in the water tetramer cations after ionization. Additionally, the PT rate is strongly dependent on the structural form of $(H_2O)_4$. To elucidate the generality of these features, the ionization processes of a water hexamer with a cage structure were examined in the same manner. Figure 6 shows a sample trajectory of a long-lived intermediate complex. The neutral water cluster was composed of six water molecules with a cage structure.

The protons of W1 orient towards the W2 and W3 molecules, and after vertical ionization, the hole was mainly localized on W1 at time zero. An intermediate complex with a symmetric structure, H_2O(W2)-H_2O^+(W1)-H_2O(W3), was formed at 25 fs. The molecular distances of W1-W2 and W1-W3 were calculated to be 2.589 and 2.557 Å, respectively, at 53.2 fs. At 80.3 fs, the symmetry of the structure was broken (the molecular distances became 1.880 and 2.066 Å, respectively), and the proton of W1 was immediately transferred to W2 at 110 fs. Thus, the H_3O^+(W2)-OH (W1) complex was completely formed. In this case, the long-lived intermediate complex with a symmetric core structure and the branched form of $(H_2O)_4$ were formed.

4. Discussion

A. **Reaction model**

The reaction model proposed in this work is schematically illustrated in Figure 7. Figure 7A shows the normal hydrogen bond network. The water molecule in the central position has a dangling proton, and the fast PT occurs after ionization. In contrast, a case of slow PT is shown in Figure 7B. The two protons of the central water molecule bind equivalently to the two water molecules on both sides, and thus, PT cannot occur. After ionization, the symmetric cation core is formed, which is the basis for the long-lived complex.

B. **Final remarks**

The present calculations revealed that the reaction processes in the branched and cyclic water tetramers differ significantly from each other. In the cyclic form, fast PT was observed after vertical ionization, and OH dissociation occurred after the second PT.

The PT reaction rate was calculated to be ca. 10 fs. In contrast, a long-lived intermediate was noted in the ionization of the branched form, in which the core H_2O^+ ion is surrounded by two water molecules. PT occurs at 130 fs, which is about 10 times slower than that of the cyclic form. These results suggest that the core H_2O^+ ion (two orientations) may exist as a long-lived intermediate complex in bulk water clusters. No OH dissociation was observed in the branched form.

We proposed here the formation model of long-lived intermediate complex. This model is only effective for the gas phase cluster. In bulk water and ice, another mechanism may be necessary because the symmetry of the bridge water is rapidly broken in large number of water molecules. The calculation of the further large system would be necessary to check the validity of this model.

In the present study, the structure of $(H_2O)_4$ was fluctuated on the potential energy surface obtained at the B3LYP/6-311++G(d,p) level. To check the validity of B3LYP functional, the geometry and vibrational frequencies of $(H_2O)_4$ obtained by the B3LYP were compared with those of MP2 calculation. Additionally, direct AIMD calculations of $(H_2O)_4^+$ were carried out from the B3LYP and MP2 optimized geometries for comparison.

The results of optimized structures, vibrational frequencies, and time evolution of potential energy were given in supporting information. The AIMD calculations revealed that the B3LYP geometry gave the reasonable dynamics for $(H_2O)_4^+$. Hence, the B3LYP is consistent with the MP2 results.

Acknowledgment. The author acknowledges partial support from JSPS KAKENHI Grant Number 15K05371 and MEXT KAKENHI Grant Number 25108004.

References

[1] K. Mizuse, J-L. Kuo, A. Fujii, Structural trends of ionized water networks: Infrared spectroscopy of water cluster radical cations $(H_2O)_n^+$ (n = 3–11), Chem. Sci. 2 (2011) 868.

[2] K. Mizuse, A. Fujii, Characterization of a Solvent-Separated Ion-Radical Pair in Cationized Water Networks: Infrared Photodissociation and Ar-Attachment Experiments for Water Cluster Radical Cations $(H_2O)_n^+$ (n=3-8), J. Phys. Chem. A, 117 (2013) 929.

[3] H. Do, N.A. Besley, Structure and Bonding in Ionized Water Clusters, J. Phys. Chem. A, 117 (2013) 5385.

[4] J. D. Herr, J. Talbot, R.P. Steele,

Structural Progression in Clusters of Ionized Water, $(H_2O)_{n=1-5}^+$, J. Phys. Chem. A, 119 (2015) 752.

[5] J.P. Torres-Papaqui, R. Coziol, R.A. Ortega-Minakata, THE STAR FORMATION HISTORY AND CHEMICAL EVOLUTION OF STAR-FORMING GALAXIES IN THE NEARBY UNIVERSE, Astrophys. J., 754 (2012) 144.

[6] M. Colin-Garcia, A.Heredia, A. Negron-Mendoza, Adsorption of HCN onto sodium montmorillonite dependent on the pH as a component to chemical evolution, Int. J. Astrobiology, 13 (2014) 310.

[7] H. R. Jacobson, T. Thanathibodee, A. Frebel, THE CHEMICAL EVOLUTION OF PHOSPHORUS, Astrophys J. Lett., 796 (2014) L24.

[8] V. Vaida, Perspective: Water cluster mediated atmospheric chemistry, J. Chem. Phys., 135 (2011) 020901.

[9] Y. Miller, J.L. Thomas, D.D. Kemp, B.J. Finlayson-Pitts, M.S. Gordon, D.J. Tobias, R.B. Gerber, Structure of Large Nitrate−Water Clusters at Ambient Temperatures:

Simulations with Effective Fragment Potentials and Force Fields with Implications for Atmospheric Chemistry, J. Phys. Chem. A, 113 (2009) 12805.

[10] H.T. Liu, J.P. Muller, M. Beutler, M. Ghotbi, F. Noack, W. Radloff, N. Zhavoronkov, C.P. Schulz, I.V. Hertel, Ultrafast photo-excitation dynamics in isolated, neutral water clusters, J. Chem. Phys. 134 (2011) 094305.

[11] W.S. Sheu, M.F. Chiou, Potential Energy Surface of O_2−(H_2O) and Factors Controlling Water-to-O_2^- Binding Motifs, J. Phys. Chem. A, 115 (2011) 99.

[12] E. Livshits, R. S. Granot, R. Baer, A Density Functional Theory for Studying Ionization Processes in Water Clusters, J. Phys. Chem. A, 115 (2011) 5735.

[13] A. Golan, M. Ahmed, Ionization of Water Clusters Mediated by Exciton Energy Transfer from Argon Clusters, J. Phys. Chem. Lett., 3 (2012) 458.

[14] D. Kina, A. Nakayama, T. Noro, T. Taketsugu, M.S. Gordon, Ab Initio QM/MM Molecular Dynamics Study on the Excited-State Hydrogen Transfer of 7-Azaindole in Water Solution, J. Phys. Chem. A, 112 (2008) 9675.

[15] R.M. Shields, B. Temelso, K.A. Archer, T.E. Morrell, G.C. Shields, Accurate Predictions of Water Cluster Formation, $(H_2O)_{n=2-10}$, J. Phys. Chem. A, 114 (2010) 11725.

[16] M. Kaledin, C.A. Wood, Ab Initio Studies of Structural and Vibrational Properties of Protonated Water Cluster $H_7O_3^+$ and Its Deuterium Isotopologues: An Application of Driven Molecular Dynamics, J. Chem. Theor. Comput., 6 (2010) 2525.

[17] Y.M. Wang, J.M. Bowman, Communication: Rigorous calculation of dissociation energies (D_0) of the water trimer, $(H_2O)_3$ and $(D_2O)_3$, J. Chem. Phys., 135 (2011) 131101.

[18] H.M. Lee, K.S. Kim, Water trimer cation, Theor. Chem. Acc. 130 (2011) 543.

[19] J. Ceponkus, P. Uvdal, B. Nelander, On the structure of the matrix isolated water trimer, J. Chem. Phys., 134 (2011) 064309.

[20] M. Pincua, R.B. Gerber, Hydration of cellobiose: Structure and dynamics of cellobiose –$(H_2O)_n$, n = 5–25, Chem. Phys. Lett., 531 (2012) 52.

[21] M. Jieli, M. Aida, Classification of OH Bonds and Infrared Spectra of the Topology-Distinct Protonated Water Clusters $H_3O^+(H_2O)_{n-1}$ ($n \leq 7$), J. Phys. Chem. A, 113 (2009) 1586.

[22] N.I. Hammer, J.R. Roscioli, M.A. Johnson, Identification of Two Distinct Electron Binding Motifs in the Anionic Water Clusters: A Vibrational Spectroscopic Study of the $(H_2O)_6^-$ Isomers, J. Phys. Chem. A, 109 (2005) 7896.

[23] H. Shinohara, N. Nishi, N. Washida, Photoionization of water clusters at 11.83 eV: Observation of unprotonated cluster ions $(H_2O)^+_n$ ($2 \leq n \leq 10$), J. Chem. Phys., 84 (1986) 5561.

[24] H. Shiromaru, Y. Achiba, K. Kimura, Y.T., Lee, Determination of the carbon-hydrogen bond dissociation energies of ethylene and acetylene by observation of the threshold energies of proton formation by synchrotron radiation, J. Phys. Chem., 91 (1987) 17.

[25] H. Shiromaru, H. Shinohara, N. Washida, H.S. Yoo, K. Kimura, Synchrotron radiation measurements of appearance potentials for $(H_2O)_2^+$, $(H_2O)_3^+$,$(H_2O)_2H^+$ and $(H_2O)_3H^+$ in supersonic jets, Chem. Phys. Lett., 141 (1987) 7.

[26] H. Shiromaru, H. Suzuki, H. Sato, S. Nagaoka, K. Kimura, Synchrotron radiation study on small binary molecular clusters: argon-water and carbon dioxide-water systems, J. Phys. Chem., 93 (1989) 1832.

[27] R.N. Barnett, U. Landman, Structure and Energetics of Ionized Water Clusters:

$(H_2O)_n^+$, n = 2−5, J. Phys. Chem. A, 101 (1997) 164.

[28] H. Tachikawa, Ionization dynamics of a water dimer: specific reaction selectivity , Phys. Chem. Chem. Phys., 13 (2011) 11206.

[29] H. Tachikawa, T. Takada, Ionization dynamics of the water trimer: A direct ab initio MD study, Chem. Phys., 415 (2013) 76.

[30] M. J. Frisch, G. W. Trucks, H. B. Schlegel, G. E. Scuseria, M. A. Robb, J. R. Cheeseman, G. Scalmani, V. Barone, B. Mennucci, G. A. Petersson, H. Nakatsuji, M. Caricato, X. Li, H. P. Hratchian, A. F. Izmaylov, J. Bloino, G. Zheng, J. L. Sonnenberg, M. Hada, M. Ehara, K. Toyota, R. Fukuda, J. Hasegawa, M. Ishida, T. Nakajima, Y. Honda, O. Kitao, H. Nakai, T. Vreven, J. A. Montgomery, Jr., J. E. Peralta, F. Ogliaro, M. Bearpark, J. J. Heyd, E. Brothers, K. N. Kudin, V. N. Staroverov, R. Kobayashi, J. Normand, K. Raghavachari, A. Rendell, J. C. Burant, S. S. Iyengar, J. Tomasi, M. Cossi, N. Rega, J. M. Millam, M. Klene, J. E. Knox, J. B. Cross, V. Bakken, C. Adamo, J. Jaramillo, R. Gomperts, R. E. Stratmann, O. Yazyev, A. J. Austin, R. Cammi, C. Pomelli, J. W. Ochterski, R. L. Martin, K. Morokuma, V. G. Zakrzewski, G. A. Voth, P. Salvador, J. J. Dannenberg, S. Dapprich, A. D. Daniels, O. Farkas, J. B. Foresman, J. V. Ortiz, J. Cioslowski, and D. J. Fox, Gaussian, Inc., Wallingford CT, 2009. Gaussian 09, Revision D.01, Gaussian, Inc., Wallingford CT, 2009.

[31] H. Tachikawa, Alkali metal mediated C-C bond coupling reaction, J. Chem. Phys. 142 (2015) 064301.

[32] H. Tachikawa, T. Takada, Proton transfer rates in ionized water clusters $(H_2O)_n$ (n=2-4), RSC Adv., 5 (2015) 6945.

[33] H. Tachikawa, Mechanism of Dissolution of a Lithium Salt in an Electrolytic Solvent in a Lithium Ion Secondary Battery: A Direct Ab Initio Molecular Dynamics (AIMD) Study, ChemPhysChem. 15 (2014) 1604.

[34] H. Tachikawa, Collision Induced Complex Formation following Electron Capture

of SO_2-H_2O Complex Interacting with Argon Atoms, J. Phys. Chem. A, 115(2011) 9091.

[35] H. Tachikawa, T. Fukuzumi, Ionization dynamics of aminopyridine dimer: a direct ab initio molecular dynamics (MD) study, Phys. Chem. Chem. Phys., 13 (2011) 5881.

[36] Direct AIMD code is made by our group.

[37] H. Tachikawa, Electronic states of hydrogen atom trapped in diamond lattice, Chem. Phys. Lett., 513 (2011) 94.

[38] H.J.C. Berendsen, J.PM. Postma, W.F. Vangunsteren, A. Dinola, J.R. Haak, Molecular dynamics with coupling to an external bath, J. Chem. Phys., 81 (1984) 3684.

[39] A.K. Sieradzan, Introduction of Periodic Boundary Conditions into UNRES Force Field, J. Comput. Chem., 36 (2015) 940.

[40] H.C. Cheng, C.F. Yu, W.H. Chen, Size, Temperature, and Strain-Rate Dependence on Tensile Mechanical Behaviors of Ni_3Sn_4 Intermetallic Compound Using Molecular Dynamics Simulation, J. Nanomater. 98 (2014) 214510.

[41] H. Hu, H.Y. Liu, Pitfall in Quantum Mechanical/Molecular Mechanical Molecular Dynamics Simulation of Small Solutes in Solution, J. Phys. Chem. B., 117 (2013) 6505.

[42] Tachikawa and Kawabata, Molecular Design of Ionization-Induced Proton Switching Element Based on Fluorinated DNA Base Pair, J. Phys. Chem. A, 2016, 120, 1529–1535.

Figure Captions

Figure 1 (Color On-line). (A) Optimized structure and geometrical parameters of the branched water tetramer $(H_2O)_4$. (B) The spatial distribution indicates the spin orbital of the water tetramer cation at the vertical ionization point of $(H_2O)_4$ calculated at the MP2/6-311++G(d,p) level. Bond lengths and angles are in Å and degrees, respectively.

Figure 2 (Color On-line). Snapshots of the branched water tetramer cation $(H_2O)_4^+$ after vertical ionization from the neutral state (the optimized structure obtained at the MP2/6-311++G level) calculated as a function of time. Bond lengths are in Å. The direct AIMD calculation was carried out at the MP2/6-311++G level.

Figure 3 (Color On-line). Time evolutions of the potential energies of (A) the branched water tetramer and (B) the cyclic water tetramer after vertical ionization from the neutral state.

Figure 4 (Color On-line). Optimized structure and geometrical parameters of (A) the linear water trimer, (B) the intermediate complex $(H_2O)_3^+$, and (C) the intermediate complex $(H_2O)_4^+$. Values were calculated at the MP2 and MP4SDQ/6-311++G(d,p) levels. Bond lengths and angles are in Å and degrees, respectively.

Figure 5 (Color On-line). Time evolution of the potential energies of the linear water trimer after vertical ionization from the neutral state.

Figure 6 (Color On-line). Snapshots of the cage-type water hexamer cation, $(H_2O)_6^+$, after vertical ionization from the neutral state calculated as a function of time.

Figure 7 (Color On-line). Model of the ionization of a water tetramer constructed based on the present dynamics calculations: (A) normal hydrogen bond network and (B) hydrogen bond network with the bridge water.

Figure 1.

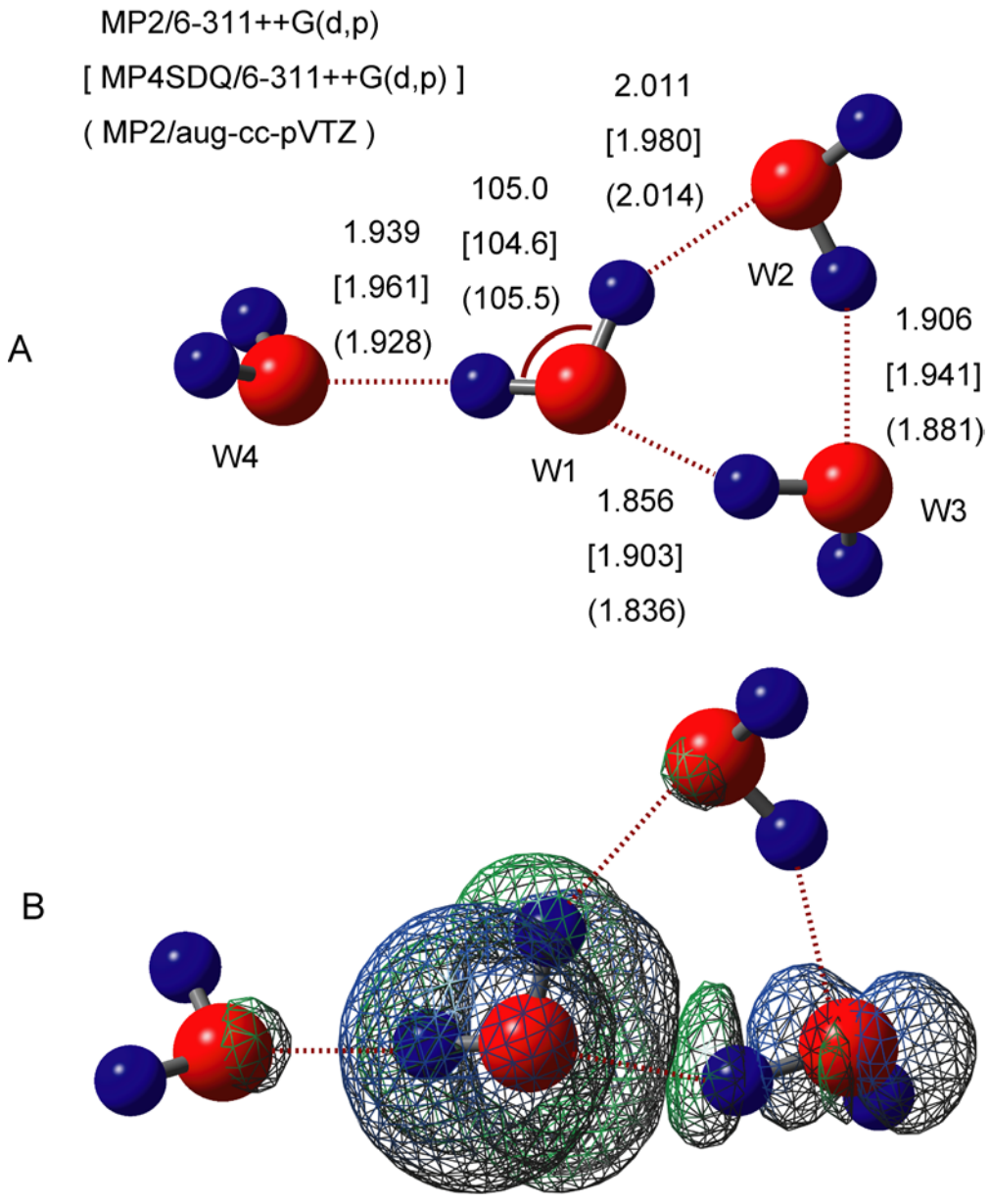
MP2/6-311++G(d,p)
[MP4SDQ/6-311++G(d,p)]
(MP2/aug-cc-pVTZ)
A
B
2.011
[1.980]
(2.014)
105.0
[104.6]
(105.5)
1.939
[1.961]
(1.928)
1.906
[1.941]
(1.881)
1.856
[1.903]
(1.836)
W1
W2
W3
W4

Figure 2.

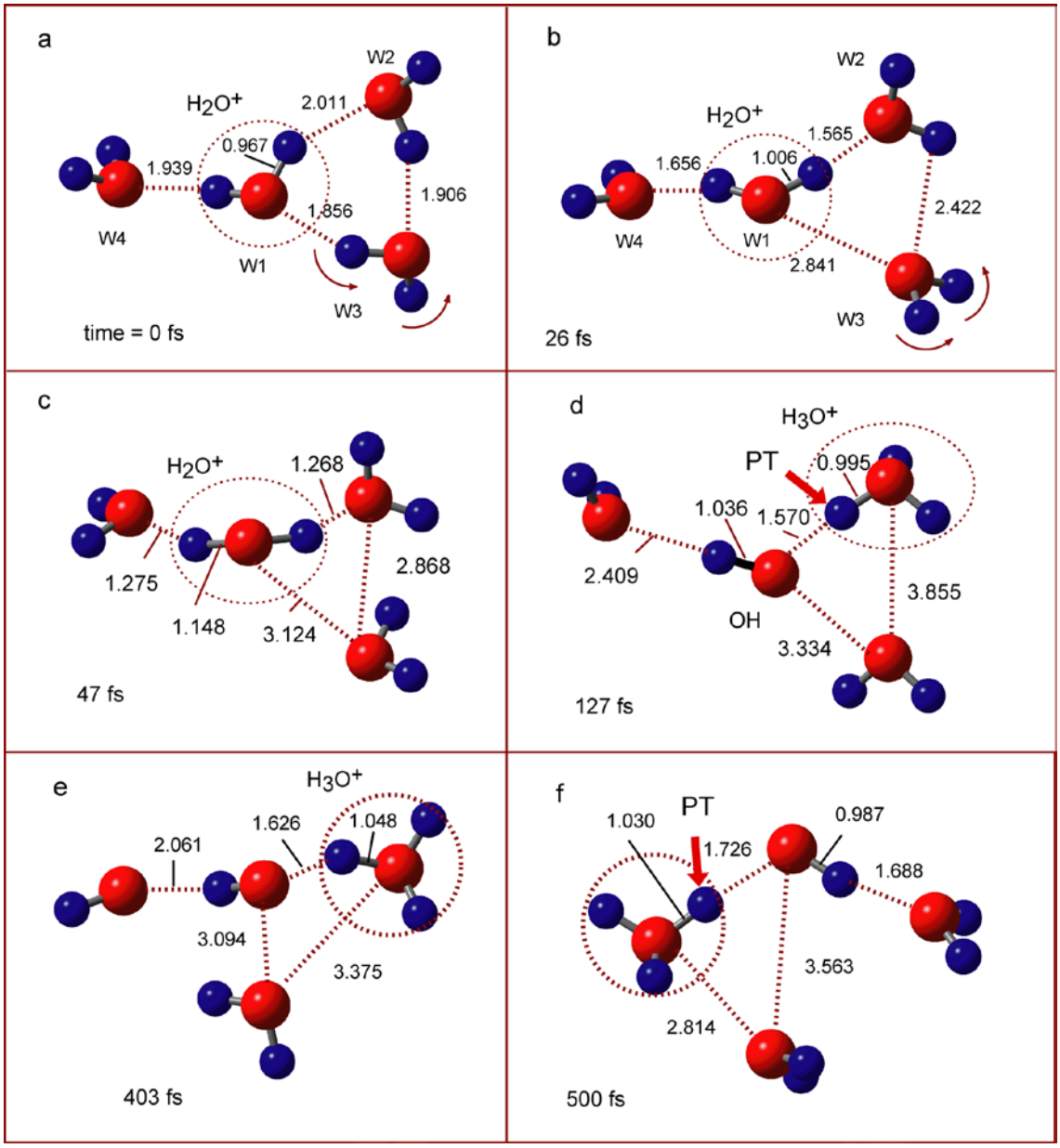
a
W2
H2O+
2.011
0.967
1.939
1.906
1.856
W4
W1
W3
time = 0 fs
b
W2
H2O+
1.565
1.656
1.006
2.422
W4
W1
2.841
W3
26 fs
c
H2O+
1.268
2.868
1.275
1.148
3.124
47 fs
d
H3O+
PT
0.995
1.036
1.570
2.409
3.855
OH
3.334
127 fs
e
H3O+
1.626
1.048
2.061
3.094
3.375
403 fs
f
PT
1.030
0.987
1.726
1.688
3.563
2.814
500 fs

Figure 3.

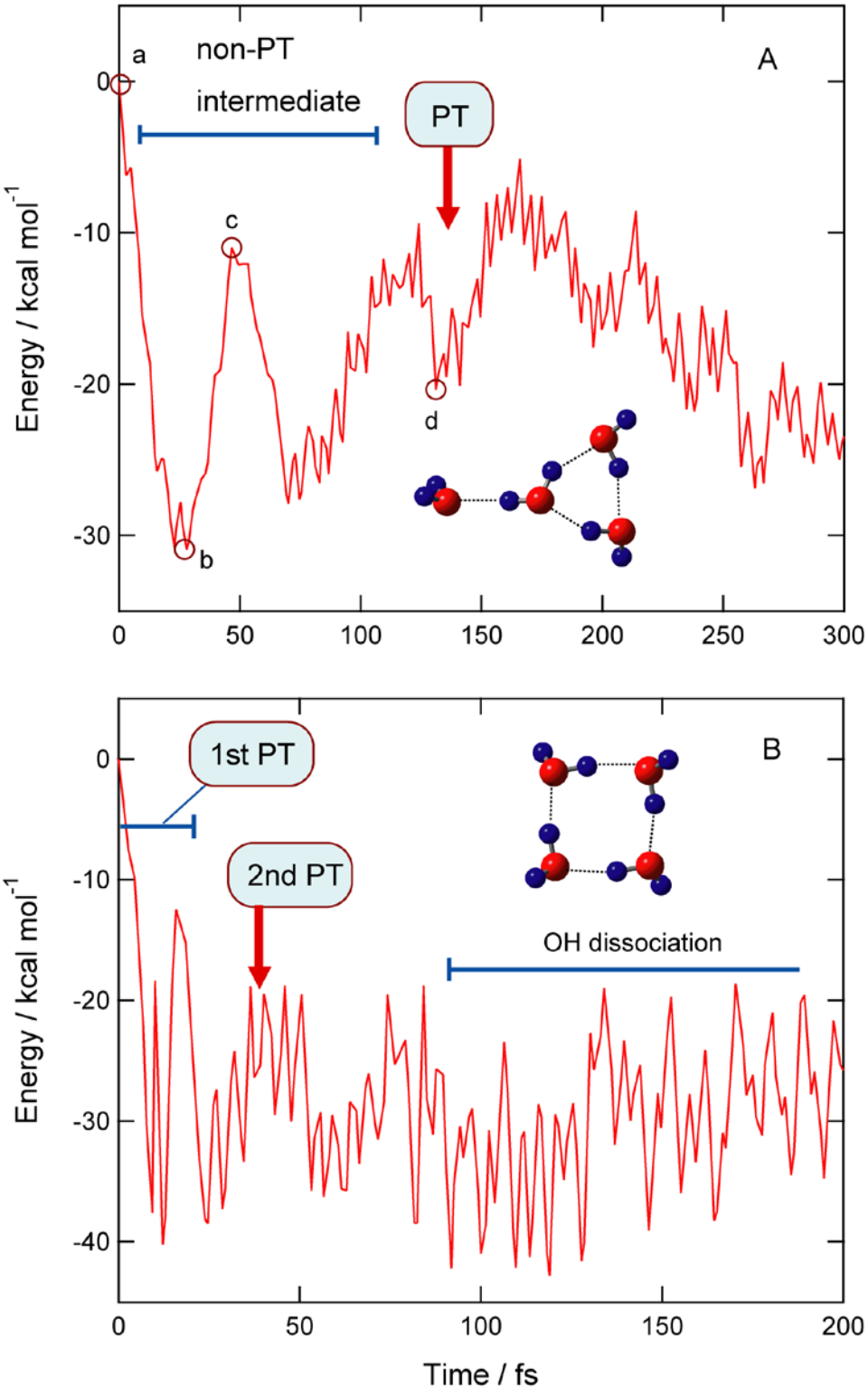
a
non-PT
intermediate
PT
A
c
b
d
Energy / kcal mol-1
0
-10
-20
-30
0
50
100
150
200
250
300
1st PT
2nd PT
B
OH dissociation
-40
Time / fs

Figure 4.

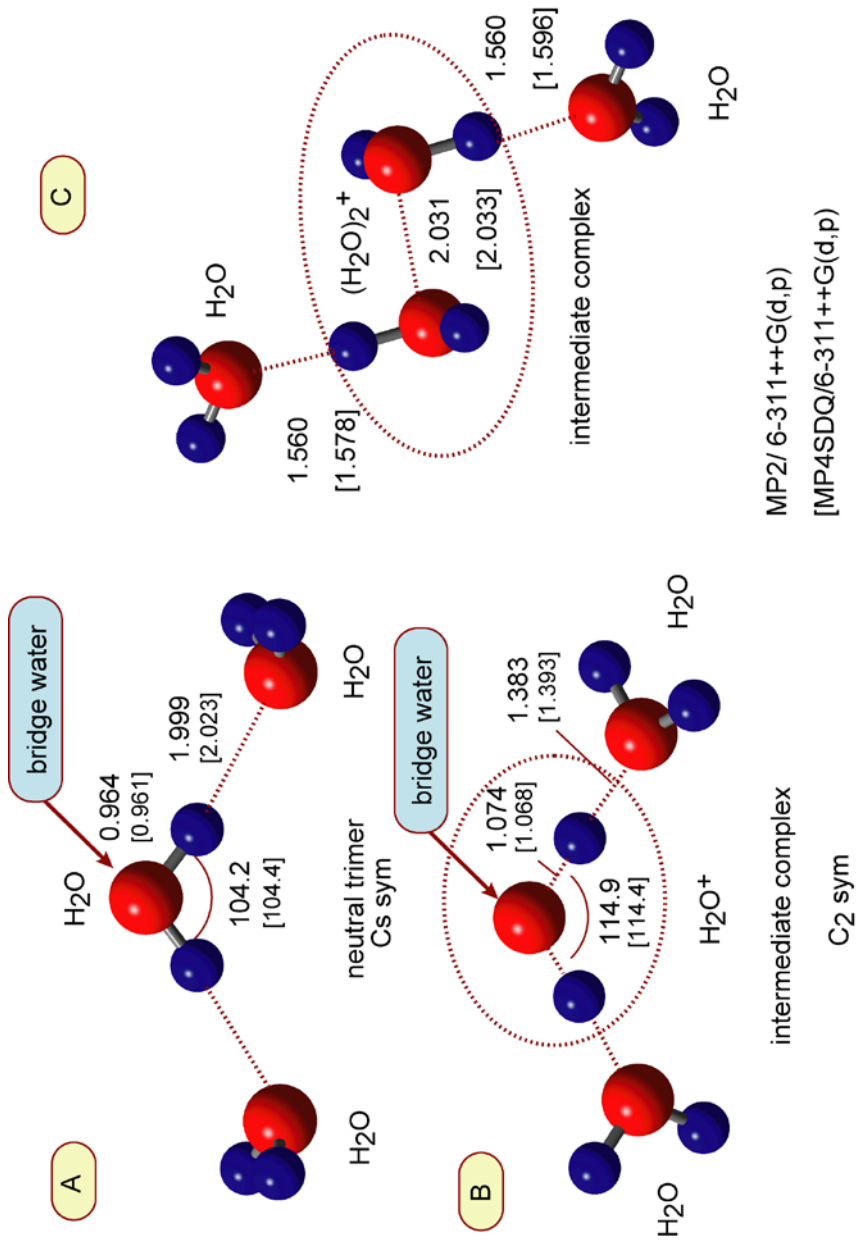
C
H2O
1.560
[1.578]
(H2O)2+
2.031
[2.033]
1.560
[1.596]
H2O
intermediate complex
MP2/ 6-311++G(d,p)
[MP4SDQ/6-311++G(d,p)
A
bridge water
H2O
0.964
[0.961]
1.999
[2.023]
104.2
[104.4]
H2O
neutral trimer
Cs sym
B
bridge water
1.074
[1.068]
1.383
[1.393]
114.9
[114.4]
H2O+
H2O
H2O
intermediate complex
C2 sym

Figure 5.

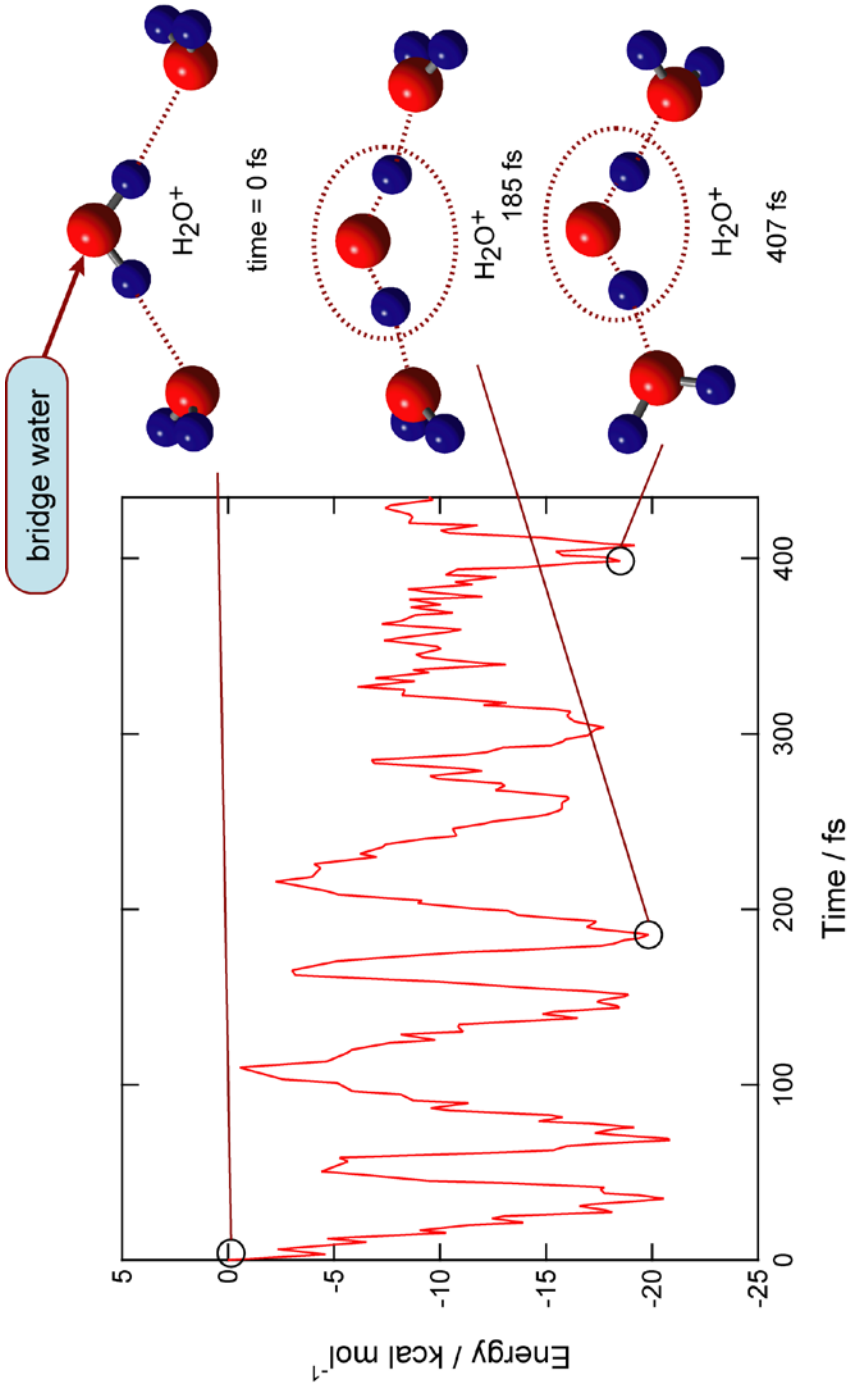
bridge water
H2O+
time = 0 fs
H2O+
185 fs
H2O+
407 fs
Energy / kcal mol-1
5
0
-5
-10
-15
-20
-25
0
100
200
300
400
Time / fs

Figure 6.

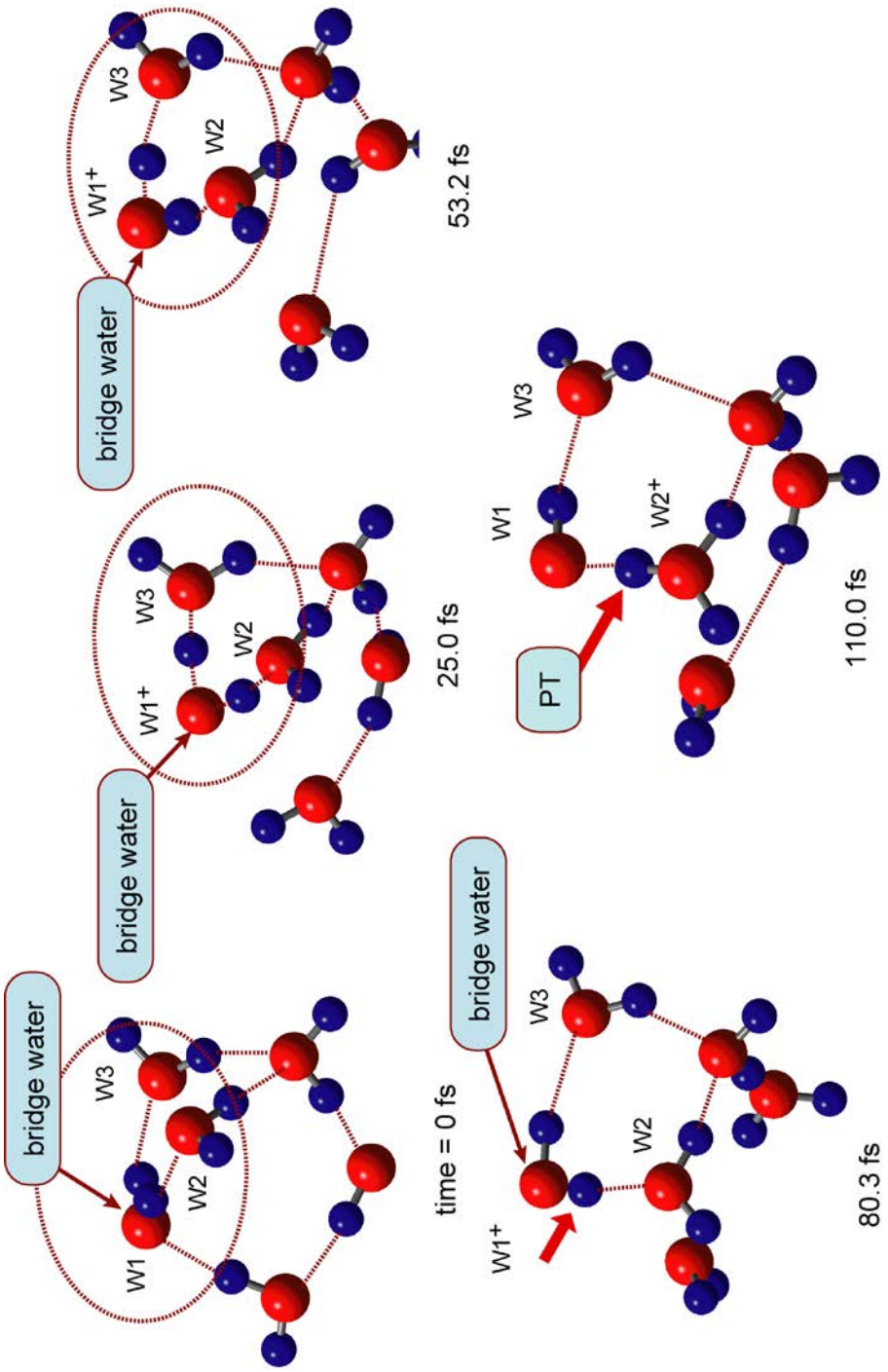
bridge water
W3
W2
W1
time = 0 fs
bridge water
W3
W2
W1+
25.0 fs
bridge water
W3
W2
W1+
53.2 fs
PT
W3
W1
W2+
110.0 fs
W1+
W2
W3
80.3 fs

Figure 7.

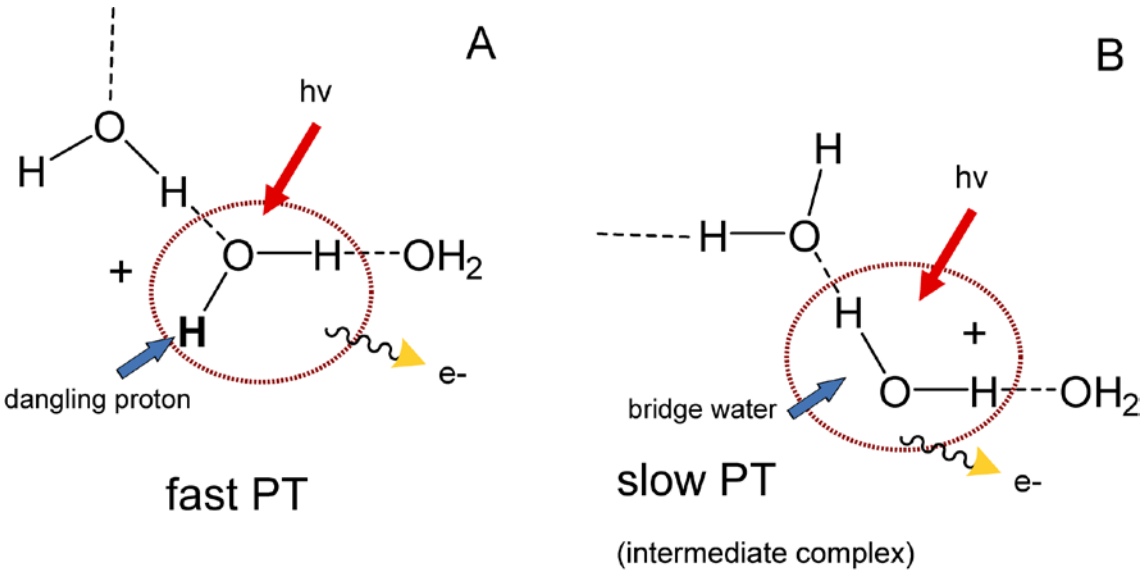
A
hv
O
H
H
+
O—H---OH2
H
dangling proton
e-
fast PT
B
H
hv
H—O
H
+
bridge water
O—H---OH2
e-
slow PT
(intermediate complex)

Graphical Abstract

.

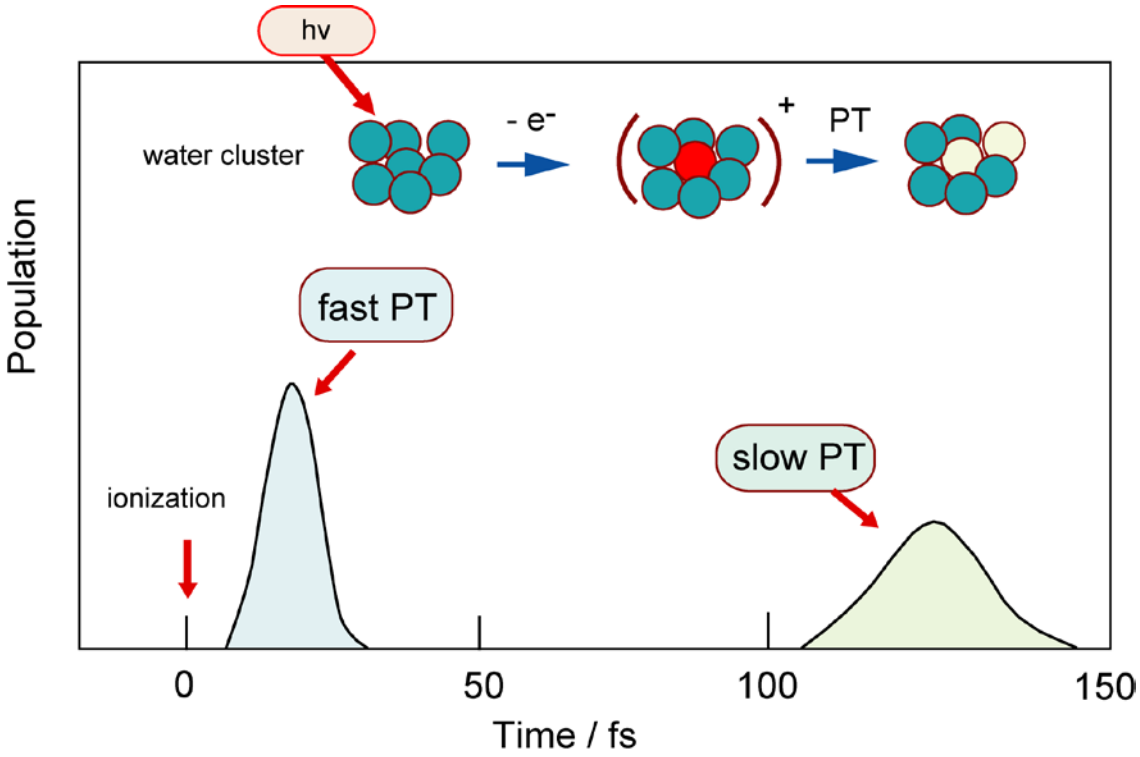

Highlights

> Two types of proton transfer (PT) processes were observed in water tetramer cations.
> Varying the topological conformation affected the PT reaction rate.
> Ionizing the cyclic water tetramer resulted in fast PT without an intermediate.
> Branched tetramers lead to the formation of long-lived non-PT intermediates.